Available online at www.sciencedirect.com
ScienceDirect
Acta Materialia 59 (2011) 1456–1463
Acta MATERIALIA
www.elsevier.com/locate/actamat

Atomic-scale simulation of screw dislocation/coherent twin boundary interaction in Al, Au, Cu and Ni

M. Chassagne [a,b], M. Legros [a], D. Rodney [b,*]

[a] CEMES, CNRS, 29 rue Jeanne Marvig, 31055 Toulouse, France
[b] SIMAP-GPM2, Grenoble INP, CNRS/UJF, 101 rue de la Physique, BP 46, 38402 Saint Martin d'Hères, France

Received 31 August 2010; received in revised form 1 November 2010; accepted 3 November 2010
Available online 7 December 2010

Abstract

The influence of material and choice of interatomic potential on the interaction between an $a/2\langle 1\,1\,0\rangle\{1\,1\,1\}$ screw dislocation and a $\Sigma 3\{1\,1\,1\}\langle 1\,1\,0\rangle$ coherent twin boundary (CTB) is determined by simulating this process in a range of face-centered cubic metals modeled with a total of 10 embedded-atom method (EAM) potentials. Generalized stacking fault energies are computed, showing a linear relation between the stacking faut (γ_S) and twin energies, as well as between the unstable stacking fault (γ_{US}) and unstable twinning (γ_{UT}) energies. We show that the reaction mechanism (absorption of the dislocation into the CTB or transmission into the twinned region) and reaction stress depend strongly on the potential used, even for a given material and are controlled by the material parameter $\gamma_S/\mu b_P$ (where μ is the shear modulus and b_P the Shockley partial Burgers vector), rather than the sign of the ratio $(\gamma_{US}-\gamma_S)/(\gamma_{UT}-\gamma_S)$, as proposed recently by Jin et al. [1]. Moreover, there exists a critical reaction stress, close to 400 MPa, independent of the potential, below which the dislocation is absorbed in the CTB and above which the dislocation is transmitted into the twinned region. The simulations are discussed with respect to *in situ* transmission electron microscopy straining experiments in Cu that highlight the importance of thermally activated cross-slip in the interaction process and show that transmission across a twin boundary is possible but is most likely an indirect process.

Keywords: Twin boundary; Dislocation; Plasticity; Molecular dynamics; *In situ* TEM

1. Introduction

The study of the interaction between slip and twins began in the 1960s with the work of Sleeswyk and Verbaak in body-centered cubic (bcc) crystals [2] and was extended to face-centered cubic (fcc) crystals by Mahajan and Chin [3] (see Refs. [4,5] for reviews). Interest in the interaction of dislocations with coherent twin boundaries (CTBs), of the type $\Sigma 3\{1\,1\,1\}\langle 1\,1\,0\rangle$, was renewed recently when it was shown that the introduction of nanoscale growth twins (thickness in the range 10–100 nm) in electrodeposited Cu (average grain size ~400 nm) allows a high tensile strength (~1 GPa) while retaining a high tensile ductility (~13%) [6,7]. Similar strengthening was also reported in austenitic stainless steels [8].

Atomic-scale computer investigations of the interaction between dislocations and CTBs were first performed in simple bicrystal geometries [8,1,9–11] and later in large-scale molecular dynamics (MD) simulations of plasticity in twinned nanocrystals [12–18]. In bicrystals, the most comprehensive study was performed by Jin et al. [1,11] who simulated in quasi-two dimensions the interaction between lattice dislocations and CTBs. For this geometry, there are only three non-equivalent dislocation configurations: a screw dislocation and two 60° mixed dislocations with either a 30° or 90° leading Shockley partial. MD simulations were performed at very low temperature (<10 K) with the dislocation driven into the CTB by an applied shear strain imposed in a single increment (i.e. from 0 to the desired applied strain). The screw dislocation will be

* Corresponding author. Tel.: +33 4 76 82 63 37; fax: +33 4 76 83 63 62.
E-mail address: david.rodney@grenoble-inp.fr (D. Rodney).
URL: http://drodneygroup.webs.com (D. Rodney).

1359-6454/$36.00 © 2010 Acta Materialia Inc. Published by Elsevier Ltd. All rights reserved.
doi:10.1016/j.actamat.2010.11.007

of particular interest in the present paper. It was studied by Jin et al. in three fcc metals (Al, Cu and Ni) modeled with embedded-atom method (EAM) potentials. The simulations showed that the dislocation/CTB interaction is systematically repulsive at large distance [10]. At short distance, depending on the material, the interaction may either become attractive (in the case of Al) leading to spontaneous absorption of the dislocation into the CTB [19] or remains repulsive (in the case of Cu and Ni). In the latter case, the leading Shockley partial comes into contact with the CTB and no reaction occurs until the applied strain is high enough to constrict the dislocation. This condition of constriction prior to reaction, similar to the Friedel–Escaig mechanism for cross-slip [20], contrasts with the Peierls models of dislocation/coherent interfaces that predict a progressive transmission of slip [21,22]. After constriction, the dislocation may either cross-slip and be absorbed into the CTB, resulting in the migration of the latter by one atomic plane, or it may cut through the CTB and be transmitted into the twinned region (this latter reaction will be called direct transmission because the Burgers vector of the impeding dislocation is conserved during the reaction). The reaction depends on the material but the reaction stress was found on the order of 400 MPa in both Cu and Ni. Jin et al. proposed a criterion to discriminate between materials where absorption or direct transmission occurs, based on generalized stacking fault energies. Namely, they proposed to consider the sign of the ratio between $R = (\gamma_{US} - \gamma_S)/\mu b$ and $R' = (\gamma_{UT} - \gamma_S)/\mu\ b$, where γ_S is the intrinsic stacking fault energy, γ_{US} the unstable stacking fault energy, i.e. the energy barrier to create an intrinsic stacking fault in a perfect crystal, and γ_{UT} the unstable twin energy, i.e. the energy barrier to add a twin plane to a pre-existing twinned region (μ is the shear modulus in $\{1\,1\,1\}\langle 1\,\bar{1}\,0\rangle$ shear planes and b the lattice dislocation Burgers vector). This criterion was inspired from Rice's criterion for dislocation nucleation at a crack tip [23], which was recently extended to include twin nucleation [24].

Large-scale MD simulations in twinned nanocrystals were conducted in Cu at constant strain-rate ($\sim 10^8\ s^{-1}$) and constant temperature (in most cases 300 K). Presumably due to the high strain rate and the absence of initial dislocation density or low-stress dislocation sources, the nanocrystals yield at very high tensile stresses (2–3 GPa) and the strength is mostly controlled by the nucleation of lattice dislocations. As a result, the presence of nanotwins does not strengthen the material [13–16] and high-stress reactions not observed in bicrystal geometries were reported. In particular, Zheng et al. [13] observed the direct transmission of screw dislocations by a Fleischer mechanism [25], i.e. successive transmission of the leading and trailing Shockley partials without constriction. In addition, extensive simulations were conducted on twinned nanowires, adding the effect of free surfaces. Although Au [26,27] and Cu [28] have been the subject of particular investigation, Deng and Sansoz [29] performed a systematic study in various fcc metals modeled using several EAM potentials for each material. They showed a strong influence of the potential, such that a given material modeled with different potentials may behave very differently.

We revisit here the screw dislocation/CTB interaction in the same spirit as the work of Deng and Sansoz [29] and perform a systematic study in Al, Au, Cu and Ni modeled with various EAM potentials in order to extract trends across materials and potentials. We consider a periodic simulation cell comprising a nanotwin to impose less constraining boundary conditions than in the bicrystal geometry, while retaining the ability to apply low stresses closer to those met in experiments than in large-scale MD simulations. We perform quasistatic simulations where the load is increased in small increments to avoid inertial effects and compare three types of loading conditions to evaluate their influence on the reaction mechanism and stress. In addition to atomic-scale simulations, we also performed *in situ* transmission electron microscopy (TEM) straining experiments in Cu thin foils containing twin boundaries, in order to evaluate the realism of the simulations. These experiments show the importance of thermally activated cross-slip that is not accounted for in simulations. In the following, we first compute the relevant generalized stacking fault energies for each EAM potential used here (Section 2). We then present the screw dislocation/CTB interaction simulations and investigate the influence of the loading condition and interatomic potential (Section 3). We finally discuss the trends observed in simulations and compare them with TEM observations (Section 4).

2. Generalized stacking fault energies

We consider four fcc metals modeled with a total of 10 EAM potentials: for Al we employed the potentials developed by Ercolessi and Adams [30] and Mishin et al. [31], for Au by Grochola et al. [32], for Cu by Mishin et al. [33], Mendelev et al. [34], Ackland et al. [35] and Foiles et al. [36], and for Ni by Mishin et al. [31], Angelo et al. [37] and Chen et al. [38]. In the following, we refer to these potentials by their corresponding material and first author name; for example Cu_Mishin.

We computed, and have listed in Table 1, the material parameters of interest for the present study: b_P the Shockley partial Burgers vector, μ the $\{1\,1\,1\}\langle 1\,\bar{1}\,0\rangle$ shear modulus, γ_S the intrinsic stacking fault energy, γ_T the twin energy, i.e the CTB surface energy, γ_{US} the unstable stacking fault energy, and γ_{UT} the unstable twin energy.

2.1. Technique

Generalized stacking fault energies were evaluated by computing $\{1\,1\,1\}\langle 1\,1\,2\rangle$ γ-lines in perfect and twinned crystals made of 10 repeating cells in directions $X = [1\,1\,2]$ and $Y = [1\,\bar{1}\,0]$ and 20 in direction $Z = [1\,1\,\bar{1}]$. We checked that these dimensions are large enough to avoid finite size effects. Periodic boundary conditions are applied in direc-

Table 1
Material properties for various EAM potentials for fcc metals. The mechanism refers to the screw dislocation/CTB interaction mechanism which is either absorption (A) or direct transmission (T). The reaction stress τ_C is the last stress in the reference cell before the dislocation reacts (with a load increment of 10 MPa).

	b_P (nm)	μ (GPa)	γ_S (mJ m^{-2})	γ_T (mJ m^{-2})	γ_{US} (mJ m^{-2})	γ_{UT} (mJ m^{-2})	Mechanism	τ_C (MPa)
Al Ercolessi	0.164	32	106.0	58.1	128.3	54.4	A	0
Al Mishin	0.165	27	149.3	77.0	168.0	67.6	A	0
Au Grochola	0.166	27	42.6	21.3	91.6	57.7	A	180
Cu Mishin	0.148	41	44.7	22.4	162.0	138.9	A	300
Cu Mendelev	0.149	42	38.1	19.0	266.2	245.0	T	510
Cu Ackland	0.148	41	36.0	19.9	312.9	293.0	T	540
Cu Foiles	0.147	42	14.5	7.3	152.1	144.7	T	460
Ni Mishin	0.144	74	125.2	63.4	367.6	302.2	T	480
Ni Angelo	0.144	73	88.8	50.4	212.3	159.1	A	410
Ni Chen	0.144	73	57.5	29.7	225.9	195.4	T	620

tions X and Y while free surfaces are used in direction Z. For the twinned crystal, the lower half-crystal in direction Z is mirrored with respect to the upper half-crystal along the central $(1\,1\,\bar{1})$ plane of the simulation cell. The γ-lines are computed in the usual fashion [39]: the upper half-crystal is rigidly shifted in the $X=[1\,1\,2]$ direction parallel to the central Z-plane in small increments and out-of-plane displacements are relaxed by energy minimization for each increment, keeping the in-plane displacements constant.

2.2. Results

The results are listed in Table 1. Fig. 1 shows typical examples of γ-lines in perfect and twinned crystals, similar to those presented in Ref. [1]. The reference energy is that of the relaxed perfect crystal with no shift (thus accounting for the two free surfaces in the Z direction). The γ-line in the perfect crystal starts at zero energy, is maximum at γ_{US} and ends at γ_S when the shift equals b_P. In the twinned crystal, the γ-line is symmetrical with respect to $b_P/2$, starts and ends at γ_T and is maximum at $\gamma_T+\gamma_{UT}$. The perfect and twinned γ-lines cross at $b_P/2$, as explained in the next subsection, and since in the perfect crystal γ_{US} occurs at a shift only slightly larger than $b_P/2$, we have $\gamma_{US}\simeq\gamma_T+\gamma_{UT}$, except in Al where the difference is larger as seen in Fig. 1a.

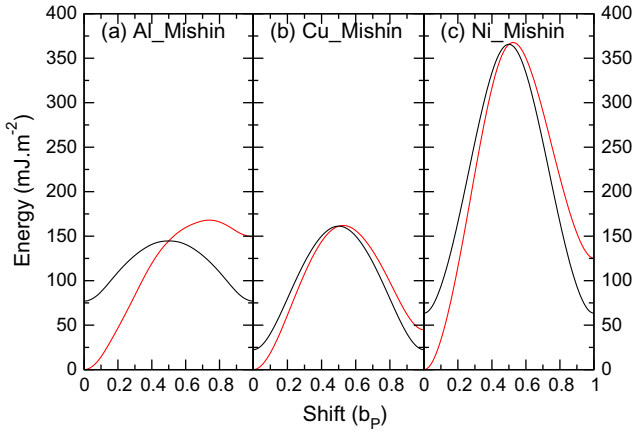

Fig. 1. $(1\,1\,\bar{1})\langle 112\rangle$ γ-lines with (a) Al_Mishin, (b) Cu_Mishin and (c) Ni_Mishin in perfect (red line) and twinned (black line) crystals. (For interpretation of the references to colour in this figure legend, the reader is referred to the web version of this article.)

2.3. Trends

Several trends are identified across the materials and interatomic potentials. First, there are large variations of fault energies for a given material depending on the potential used. This mainly comes from the fact that it is difficult to account for a high stacking fault energy within the EAM formalism. This energy, if not included in the list of fitted quantities, is systematically small compared to experimental values, as in the cases of Cu_Foiles and Ni_Chen. All potentials used here, except for the two mentioned above, were chosen because they predict reasonably high stacking fault energies compared to other potentials published in the literature (see, for example, some of the potentials used in Ref. [29]). In that respect, the potentials developed by Mishin et al. for Al, Cu and Ni are systematically close to experimental values but come at the price of having large cut-off radii, and therefore longer computing times, than other potentials.

Second, Fig. 2 shows a remarkable linear correlation between γ_T and γ_S and a looser but still relevant linear correlation between γ_{UT} and γ_{US}. Quantitatively, we have:

$$\gamma_S = 2\gamma_T, \tag{1}$$

$$\gamma_{US} \simeq \gamma_{UT} + 43. \tag{2}$$

The proportionality between γ_S and γ_T can be explained by inspecting stacking sequences. In a perfect fcc crystal, the stacking sequence of $\{1\,1\,1\}$ planes is ternary: *abcabc*, such that any plane (e.g. *a*) is surrounded on both sides and up to second neighbors by planes with a different stacking (*b* and *c*). Near a stacking fault, the stacking is binary ***a*****c** **b**|**c** **b***a* and two pairs of second-neighbor planes have the same stacking (the *c* and *b* planes in bold in the previous sequence). Planes with identical stacking imply a shorter

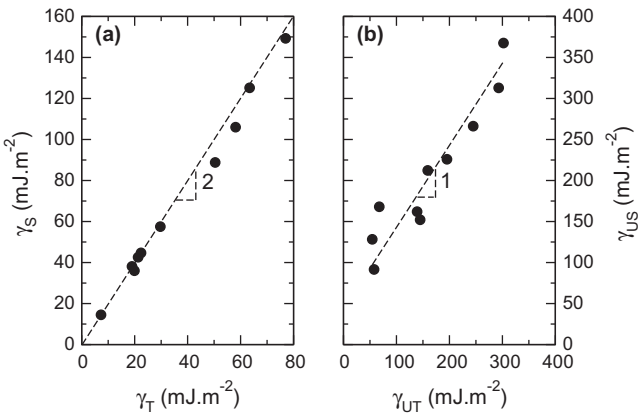

Fig. 2. Correlation among EAM potentials between (a) stacking fault energy γ_S and twin energy γ_T and (b) unstable stacking fault energy γ_{US} and unstable twin energy γ_{UT}.

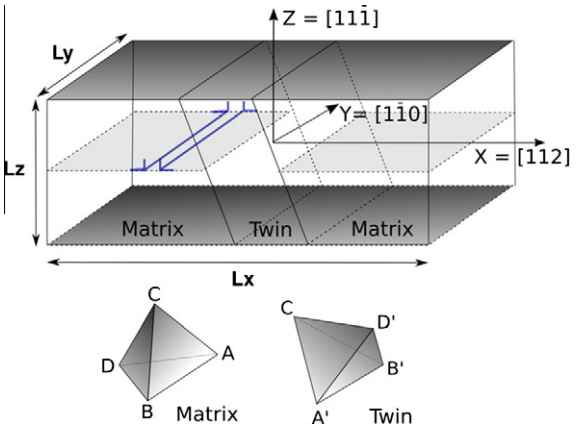

Fig. 3. Schematic representation of the simulation cell with corresponding Thompson tetrahedra showing the crystallographic orientation of the matrix and nanotwin.

separation between atom pairs compared to unlike stacking. This is the main origin of excess stacking fault energy. Near a CTB, the stacking is *cb***a**|*c***a**b, with only one pair of second-neighbor planes with same stacking (the *a* planes in bold). In the unrelaxed crystal, the energy cost of a CTB is thus half of that of an intrinsic stacking fault and Fig. 2a shows that the ratio remains almost the same after relaxation.

We mentioned above that the γ-lines in perfect and twinned crystals cross at $b_P/2$. This can also be explained by inspecting the corresponding stacking sequence. When the shift is $b_P/2$, the sequences near the fault plane are *ca bc ab*|*cba* and *ca bc ab*|*cab* in perfect and twinned crystals, respectively, where *ca* stands for the mid-position between the *c*- and *a*-planes. Up to second-neighbor planes, the two planes affected by the shift are the *ab* and *c* planes adjacent to the fault. For the *ab* plane, the second-neighbor *b* plane on the right side of the fault in the perfect crystal is replaced by an *a* plane in the twinned crystal but *a* and *b* planes are symmetrical with respect to the *ab* position. For the *c* plane, the *a* and *b* planes on the right are interchanged between perfect and twinned crystals, but this again does not affect the energy. The two stacking sequences have thus the same energy in the unrelaxed configurations and we see from Fig. 1 that this remains approximatively true after relaxation.

3. Dislocation/CTB interaction

3.1. Simulation cell

Fig. 3 shows the simulation cell used to simulate the screw dislocation/CTB interaction. In order to remain close to experimental conditions, we considered a periodic crystal (called the matrix) containing a nanotwin bordered by two CTBs. The Thompson tetrahedra in Fig. 3 show the respective crystallographic orientations of the matrix and nanotwin. Periodic boundary conditions are applied in directions $X = [1\,1\,2]$ and $Y = [1\,\bar{1}\,0]$, while the boundary condition in direction $Z = [1\,1\,\bar{1}]$ depends on the type of loading condition applied (see below in Section 3.2). Initially, a screw dislocation is introduced between the two central Z-planes along the Y-direction by means of its elastic displacement field, and periodicity is restored in direction X by adding a shift of $b/2$ in direction Y across the X-surfaces [40,41]. Along the Y-direction, the cell is quasi-two-dimensional. In direction Z, the cell height is $113a/\sqrt{3}$, where a is the lattice parameter. In direction X, we considered a reference cell length of $L = L_X = 240a\sqrt{3/2}/2$ and a reference twin width of $W = 84a\sqrt{3/2}/2$, i.e. containing 84 $\{1\,1\,1\}$ planes parallel to the CTBs. In Cu, it corresponds to a width of about 18.6 nm, which is in the range of experimental values for nanotwinned Cu. We tested the influence of these parameters by considering cells of length $2L$ and a nanotwin of width either W or $2W$.

3.2. Loading conditions

We compared three types of loading conditions resulting in either an applied shear stress τ_{YZ} or shear strain ϵ_{YZ}: (1) stress-controlled loading by applying traction forces to the atoms in slabs of width equal to the potential cut-off radius from the upper and lower Z-surfaces (for simplicity, these regions will be referred to as the Z-surfaces), the Z-surfaces are otherwise free; (2) rigid strain-controlled loading by rigidly shifting the upper and lower Z-surfaces; and (3) flexible strain-controlled loading by constraining only the motion of the center of gravity of the upper and lower Z-surfaces. This last loading condition was recently proposed [42] as a less constraining alternative to rigid boundary conditions, allowing the atoms in the upper and lower surfaces to adapt to the plastic strain produced when the dislocation glides in the simulation cell. For more details on loading conditions, the reader is referred to Ref. [41].

Stress–strain curves with the three loading conditions are shown in Fig. 4 for the Cu_Mishin potential. The curves include data recorded during the relaxations and

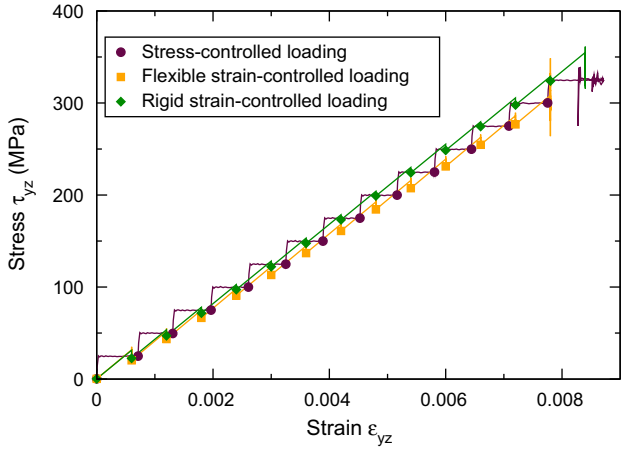

Fig. 4. Stress–strain curves for Cu_Mishin obtained with three loading conditions: stress-controlled, rigid strain-controlled and flexible strain-controlled as noted in the legend. The load increment is 25 MPa with stress control and 6×10^{-4} with strain control.

the filled symbols correspond to equilibrium configurations at the end of each loading increment. We see that rigid boundary conditions induce larger stresses at a given strain and yield a higher reaction stress than stress-controlled or flexible loading conditions. The reason is that rigid boundary conditions force the nanotwin and matrix to undergo the same average deformation, which is not the minimum-energy configuration in anisotropic crystals. Note, however, that all loading conditions yield the same reaction mechanism: absorption of the dislocation in the CTB with the present Cu_Mishin potential. These observations are common to all potentials investigated here: the three loading conditions yield the same reaction mechanism but rigid strain-controlled loading overestimates the reaction stress compared to stress-controlled and flexible strain-controlled loading conditions that are essentially equivalent.

We investigated the influence of the cell length in direction X, i.e. the periodic distance between nanotwins, and of the nanotwin width. Both parameters affect the reaction stress but not the reaction mechanism: the reaction stress decreases with the cell length and increases with the nanotwin width. The variations are, however, small, of the order of 10% for both parameters. For instance, with Cu_Mishin and stress-controlled loading, doubling L_X from 240 to $420a\sqrt{3/2}/2$ at fixed twin width ($84a\sqrt{3/2}/2$) decreases the reaction stress from 300 to 250 MPa, while with $L_X = 420a\sqrt{3/2}/2$, doubling the twin width to $168a\sqrt{3/2}/2$ increases the reaction stress to 290 MPa. We also investigated the influence of inertial effects by performing MD simulations started at 0 K with the stress or strain applied in a single increment, as in the work of Jin et al. [1]. We found that inertia favors transmission over absorption. For instance, in the case of Cu_Mishin, if 3 % strain is applied in a single increment to a relaxed configuration, the dislocation is transmitted across the CTB instead of being absorbed as obtained with smaller strain increments. In order to avoid inertial effects, the simulations discussed in the following were performed using stress-controlled loading with static relaxations and load increments of 10 MPa.

3.3. Reaction mechanisms and stresses

As reported by Jin et al. [1], the screw dislocation can be either absorbed by cross-slip in the CTB or transmitted inside the nanotwin. The case of Al is particular because with the two potentials used here, there is a stand-off distance of about 4 nm below which the CTB attracts and spontaneously absorbs the dislocation, as reported by Chen et al. [10]. In all other cases, the front Shockley partial is brought in contact with the CTB without spontaneous absorption and no reaction occurs until the stress is high enough to constrict the dislocation. The screw dislocation then either dissociates in the twinned region and is transmitted across the CTB, or is absorbed by dissociation in the CTB and forming two non-bonded Shockley partials that glide in opposite directions and progressively add a {1 1 1} plane to the nanotwin. The absence of spontaneous reaction shows that the process involves energetically unfavorable rearrangements in the CTB. In experimental conditions where dislocation pile-ups may form, stress concentrations at the CTB may allow these rearrangements [43]. Here, since there is only one dislocation, the rearrangements are triggered by the applied stress only. Reaction mechanisms and stresses in the reference cell ($L = 240a\sqrt{3/2}/2$ and $W = 84a\sqrt{3/2}/2$) are listed in Table 1. In Cu and Ni, depending on the potential used, two possible mechanisms may occur. Thus, a particular mechanism cannot be ascribed to a given material. Fig. 5 shows the reaction strain $\epsilon_C = \tau_C/\mu$ as a function of the nondimensional parameter $\gamma_S/\mu b_P$, which reflects the balance between stacking fault attraction and elastic repulsion in dissociated dislocations. The figure includes data

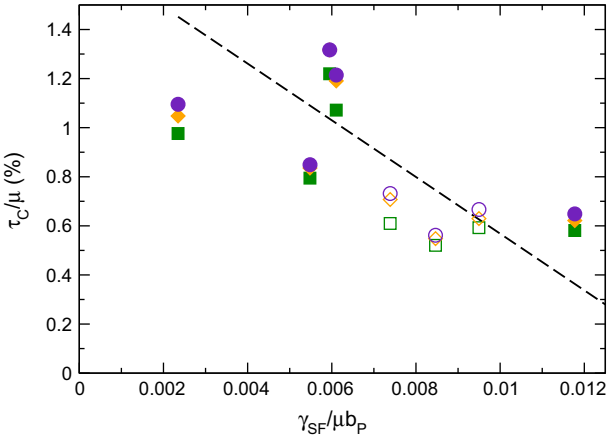

Fig. 5. Reaction strain $\epsilon_C = \tau_C/\mu$ as a function of adimensional parameter $\gamma_S/\mu b_P$ for the various potentials studied here. The straight line is the isotropic elasticity theory prediction. Open symbols correspond to absorptions in the CTB, filled symbols to direct transmission across the CTB. Circles are for the reference cell, squares for the cell twice longer with twins of reference width and diamonds for the cell twice longer with twins twice wider.

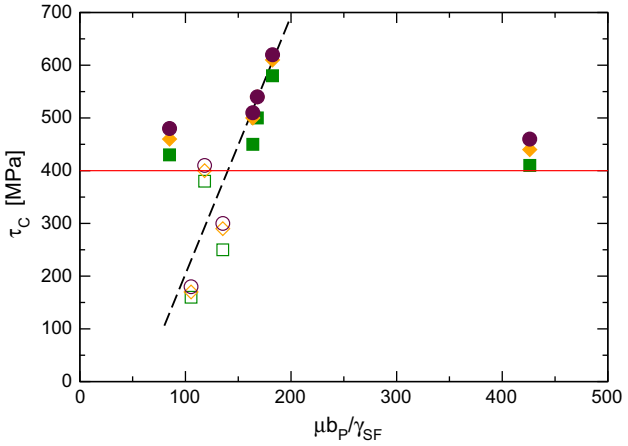

Fig. 6. Reaction stress τ_C as a function of nondimensional parameter $\mu b_P/\gamma_S$ for the various potentials studied here. The solid red line shows the critical stress below which the dislocation is absorbed in the CTB and above which it is transmitted. The dashed line is a visual guide. The same symbols as in Fig. 5 are used. (For interpretation of the references to colour in this figure legend, the reader is referred to the web version of this article.)

obtained in the reference cell as well as in cells with $2L$ and W and cells with $2L$ and $2W$. Note that data for Al where absorption is spontaneous are not shown here. From the isotropic elasticity theory of dislocations [44], the dissociation length d of a screw dislocation under a resolved shear stress $\tau = \tau_{YZ}$ is:

$$d = \frac{3\mu b_P^2}{16\pi\left(\gamma_S + \tau b_P \frac{\sqrt{3}}{2}\right)}, \tag{3}$$

with Poisson's ratio $\nu = 1/3$. If we note $\alpha = d/b_P$, the normalized dissociation distance below which a reaction can occur, Eq. (3) can be rewritten as:

$$\epsilon_C = \frac{\tau_C}{\mu} = \frac{\sqrt{3}}{8\pi\alpha} - \frac{2}{\sqrt{3}}\frac{\gamma_S}{\mu b_P}. \tag{4}$$

The straight line in Fig. 5 corresponds to Eq. (4) with $\alpha = 4$. The good agreement between elasticity theory and simulation data shows that the onset of the reaction is controlled by the dislocation constriction, i.e. the reaction stress is set by the stress required to constrict the dislocation. After constriction of the perfect dislocation, we found that direct transmission is a high-stress reaction that occurs only when the reaction stress is greater than an applied stress close to 400 MPa, independently of the potential and of cell and twin sizes. On the other hand, if constriction is reached below this critical stress, the dislocation is absorbed. This observation is illustrated in Fig. 6, which also shows a linear correlation between τ_C and $\mu b_P/\gamma_S$ with only one exception (Cu_Baskes).

4. Discussion

The present simulations show that a given reaction mechanism cannot be associated with a given material since both absorption and transmission may occur in Cu and Ni. The interaction depends more on the choice of potential than on the material, which is expected given the large scatter in material properties predicted by different potentials. The main parameter that controls both the reaction stress and mechanism is $\gamma_S/\mu b_P$, which also controls the dislocation dissociation length. An influence of the cell dimension and twin width is found, but remains small as shown in Figs. 5 and 6. In addition, the cell dimension and twin width do not affect the reaction mechanism. Jin et al. [1] proposed a criterion to predict in which materials screw dislocations are absorbed and in which they are transmitted, based on the relative sign of $R = (\gamma_{US} - \gamma_S)/\mu b$ and $R' = (\gamma_{UT} - \gamma_S)/\mu b$, absorption occurring when R'/R is negative. Inspection of Table 1 shows that the ratio is negative only for the two Al potentials, whereas absorption occurs in Cu and Ni. The criterion is therefore not adapted to discriminate between absorption and transmission but rather highlights materials where the short-range interaction is attractive, leading to spontaneous absorption. Moreover, we note that based on analogy with Rice's theory [23], Jin et al.'s criterion relates to the nucleation of a trailing partial either in the nanotwin or the CTB, whereas physically the occurrence of direct transmission or absorption depends on the emission of the leading partial since the trailing partial initially remains in the CTB.

The present simulations show that the reaction is controlled by the stress required to constrict the dislocation and direct transmission occurs when the constriction stress is larger than 400 MPa. Materials with a low $\gamma_S/\mu b_P$ parameter have therefore widely dissociated dislocations with a high constriction stress that favors transmission over absorption. At this point, the existence of a critical stress independent of the potential can only be taken as an empirical observation.

Compared to large-scale simulations of twinned nanocrystals [12–17], the stresses reported here are significantly lower and the reactions discussed here require lower stresses. In particular, we have not observed with any of the present potentials a Fleischer mechanism for direct transmission where both partials cross the CTB successively (such a mechanism was reported by Zheng et al. [13]). With all potentials, the Friedel–Escaig mechanism is observed whereby the dislocation has first to constrict before any reaction can occur.

Compared to the bicrystal simulations of Jin et al. [1], we find the same reaction mechanism in Al and Ni, but not in Cu, where we observed absorption while direct transmission was reported by the above authors. The reason is presumably that in the latter reference, the Cu_Mishin potential was refitted to reproduce 0 K properties. The new potential has a significantly lower stacking fault energy (29.5 J m^{-2}) than the original Cu_Mishin potential (44.7 J m^{-2}) with thus a lower $\gamma_S/\mu b_P$ parameter and a higher constriction stress leading to transmission. In addition, absorption as observed here is consistent with the lower activation energy for absorption than for direct

transmission computed with the original Cu_Mishin potential by Zhu et al. [9] and Chen et al. [10].

In addition to simulations, we performed *in situ* transmission electron microscopy (TEM) straining experiments on Cu thin foils containing annealing and mechanical twins. Several dislocation–twin interactions were observed with different outcomes depending on the orientation of the incoming dislocation, its Burgers vector and the "cleanliness" of the twin interface. In the situation considered in the simulations, i.e. a single incoming dislocation with a Burgers vector contained in the (1 1 1) twin plane, no direct transmission was observed. This is illustrated in Fig. 7, a typical example of such interaction. In Fig. 7a, a perfect dislocation (D) was slipping onto a (1 1 1) plane parallel to a mechanical twin before it cross-slipped onto a $(1\,1\,\bar{1})$ plane towards the twin boundary (Fig. 7b). The mechanical twin is thinner than 10 nm. The bend contours visible in the upper grain are not related to the twin, whose formation was followed during the experiment. Glide planes are identified by the traces left by the dislocation on the thin foil free surfaces (noted Tr. 1 and Tr. 2 in Fig. 7a). The fact that D is able to glide onto both (1 1 1) and $(1\,1\,\bar{1})$ planes implies that its Burgers vector is $a/2[\bar{1}\,1\,0]$ (see Fig. 7d) and is therefore contained in the twin plane. This configuration is similar to that considered in the above atomistic simulations: the dislocation has the same glide plane and Burgers vector as in Fig. 3 and is close to screw orientation since it is able to cross-slip. The outcome of the interaction in TEM is, however, different from the simulations, since D is neither absorbed nor transmitted. Instead, when the dislocation approaches the twin boundary, it cross-slips again on a (1 1 1) plane parallel to the twin boundary (Fig. 7c). The dislocation does not cross-slip in the twin plane, and is therefore not absorbed, since it would otherwise dissociate in the twin plane, adding a stacking fault to the twin that would change the α-fringe pattern seen in Fig. 7. However, the cross-slip plane must be within TEM resolution ($\sim$1 nm) since no separation between the dislocation and twin boundary is visible in Fig. 7c. Most probably, as the dislocation approached the twin under the action of the applied stress, it felt the gradually increasing elastic repulsive force produced by the twin, as reported above and in the work of Chen et al. [10], until this force was sufficient to induce cross-slip, allowing the dislocation to avoid the twin. Such reaction could not be observed in the atomistic simulations above because the latter are static and do not account for thermally activated processes, such as cross-slip.

Transmission of deformation across a twin boundary has been observed, but the *in situ* experiments highlight the difficulty of this process. An example is shown in Fig. 8 where a pile-up of dislocations had to form before transmission occurred. Fig. 8a is a video snapshot taken during the deformation. The dislocation configuration is shown schematically in Fig. 8b. A pile-up of eight dislocations moving to the right of grain 1 on a $(1\,1\,\bar{1})$ plane are densely stacked against an annealing twin that is not "clean" as in the previous case, but contains defects visible in Fig. 8a. In front of the pile-up (on dislocation 8) the stress is estimated between 100 and 150 MPa. This stress is much higher than the applied stress (on the order of 30–50 MPa, calculated from the curvature of isolated dis-

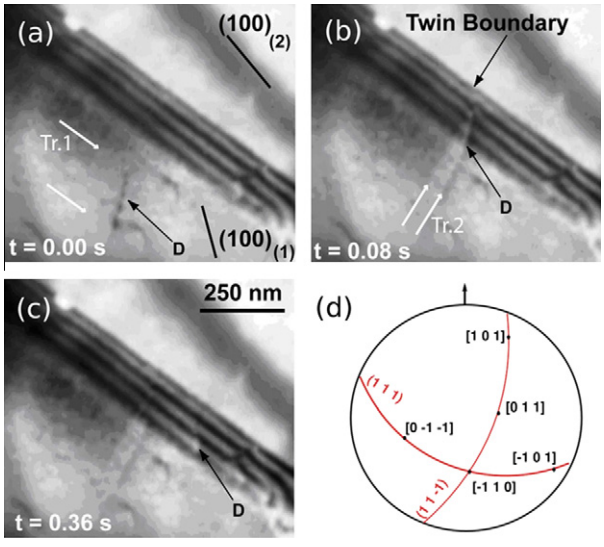

Fig. 7. Video snapshots captured during an *in situ* TEM straining experiment showing the interaction of a perfect dislocation (D) with a twin boundary. In (a), D is slipping onto a (1 1 1) plane before cross-slipping onto a $(1\,1\,\bar{1})$ plane in (b). Tr. 1 and Tr. 2 correspond to the (1 1 1) and $(1\,1\,\bar{1})$ planes, respectively. A second cross-slip of the dislocation on the (1 1 1) plane of the twin occurs in (c). In (d), the stereographic projection of grain 1 is shown.

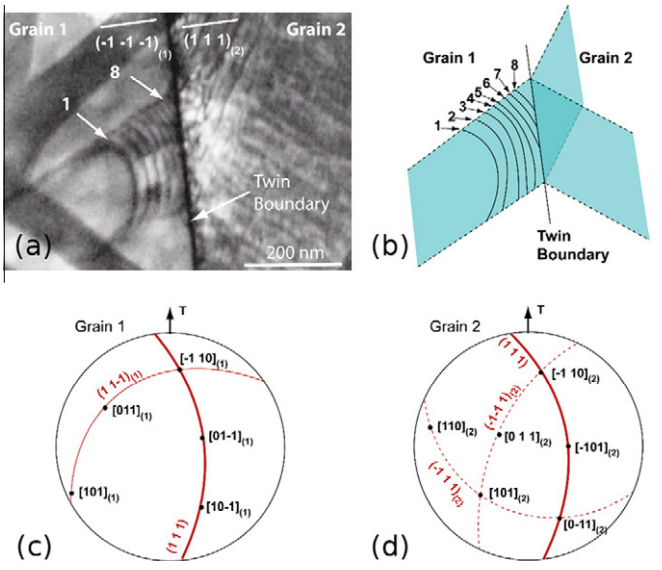

Fig. 8. *In situ* TEM straining experiment showing the emission and nucleation of dislocations across a twin boundary after a pile up has been created on the incoming side. The video snapshot is (a) is schematized in (b). The stereographic projections of grains 1 and 2 are shown in (c) and (d), respectively.

locations elsewhere in the thin foil). As seen in Fig. 8a, dislocations are emitted in grain 2 (right side of the twin boundary) on two slip planes, $(\bar{1}\,\bar{1}\,1)_{(2)}$ and $(\bar{1}\,1\,1)_{(2)}$, but they travel too fast to be captured on the video. Only their traces on the thin foil surfaces are visible. Some dislocations cross-slip in grain 2, further away from the boundary (not visible in Fig. 8a), between planes $(\bar{1}\,\bar{1}\,1)_{(2)}$ and $(1\,1\,1)$, implying that their Burgers vector is $a/2[\bar{1}\,1\,0]$, i.e. identical to the impeding dislocations. These dislocations may therefore have been directly transmitted from grain 1 to grain 2. On the other hand, the fact that a pile-up is needed suggests that this transmission is not direct. Moreover, the second activated glide plane, $(\bar{1}\,1\,1)$, cannot carry the incoming $a/2[\bar{1}\,1\,0]$ Burgers vector and therefore cannot be attributed to a direct transmission. A source of new dislocations or a reaction at the interface is therefore needed to activate this slip system. Indirect transmission of plasticity across a CTB has also been observed in copper in the case of an incoming thin twin [43]. The atomic-scale process involved in Fig. 8 is therefore more complex than reported in atomistic simulations, certainly because the annealing twin boundary considered here contains defects. Fig. 8 emphasizes the fact that no isolated dislocation has been observed to cross directly a CTB. Twin crossing is always the result of a collective process, in which the local stress is not the applied stress but is magnified by pile-up effects.

5. Conclusion

In conclusion, we have shown that even the simple configuration of interaction between an infinite screw dislocation with a CTB is a complex process that depends on the details of the interatomic potential used. No simple criterion is proposed but we found (1) that the controlling parameter is $\gamma_S/\mu b_P$, which reflects the interplay between stacking fault energy and elasticity; and (2) that there is a critical reaction stress, close to 400 MPa, below which the screw dislocation is absorbed and above which the dislocation is transmitted into the nanotwin. Further work will aim at justifying the existence of such critical reaction stress. In the case of Cu, we found that the EAM potential developed by Mishin et al. is the only Cu potential that predicts absorption of the screw dislocation. It is, however, the potential with the highest γ_S, close to experimental values, and the difficulty of direct transmission was confirmed by *in situ* TEM experiments. However, direct comparison between simulations and TEM is difficult because the simulations do not account for cross-slip or for imperfect twin boundaries.

References

[1] Jin ZH, Gumbsch P, Ma E, Albe K, Lu K, Hahn H, et al. Scripta Mater 2006;54:1163.
[2] Sleeswyk AW, Verbraak CA. Acta Metall 1961;9:917.
[3] Mahajan S, Chin GY. Acta Metall 1973;21:173.
[4] Rémy L. Metall Trans 1981;12 A:387.
[5] Christian JW, Mahajan S. Prog Mater Sci 1995;39:1.
[6] Lu L, Shen Y, Chen X, Qian L, Lu K. Science 2004;304:422.
[7] Shen YF, Lu L, Lu QH, Jin ZH, Lu K. Scripta Mater 2005;52:989.
[8] Zhang X, Misra A, Wang H, Nastasi M, Embury JD, Mitchell TE, et al. Appl Phys Lett 2004;84:1096.
[9] Zhu T, Samanta A, Kim HG, Suresh S. Proc Natl Acad Sci USA 2007;104:3031.
[10] Chen Z, Jin Z, Gao H. Phys Rev B 2007;75:212104.
[11] Jin ZH, Gumbsch P, Albe K, Ma E, Lu K, Gleiter H, et al. Acta Mater 2008;56:1126.
[12] Buehler MJ, Hartmaier A, Gao H. Model Simul Mater Sci Eng 2004;12:S391.
[13] Zheng YG, Lu J, Zhang HW, Chen Z. Scripta Mater 2009;60:508.
[14] Li L, Ghoniem NM. Phys Rev B 2009;79:075444.
[15] Shabib I, Miller RE. Model Simul Mater Sci Eng 2009;17:055009.
[16] Shabib I, Miller RE. Acta Mater 2009;57:4364.
[17] Wu ZX, Zhang YW, Srolovitz DJ. Acta Mater 2009;57:4508.
[18] Li X, Wei Y, Lu L, Lu K, Gao H. Nature 2010;464:877.
[19] Dewald MP, Curtin WA. Philos Mag 2007;87:4615.
[20] Escaig B. J Phys (Paris) 1968;29:225.
[21] Shen Y, Anderson PM. Acta Mater 2006;54:3941.
[22] Shen Y, Anderson PM. J Mech Phys Solids 2007;55:956.
[23] Rice JR. J Mech Phys Solids 1992;40:239.
[24] Tadmor EB, Hai S. J Mech Phys Solids 2003;51:765.
[25] Fleischer RL. Acta Metall 1959;7:134.
[26] Afanasyev KA, Sansoz F. Nano Lett 2007;7:2056.
[27] Deng C, Sansoz F. Nano Lett 2009;9:1517.
[28] Cao AJ, Wei YG, Mao SX. Appl Phys Lett 2007;90:151909.
[29] Deng C, Sansoz F. Acta Mater 2009;57:6090.
[30] Ercolessi F, Adams J. Europhys Lett 1994;26:583.
[31] Mishin Y, Farkas D, Mehl M, Papaconstantopoulos DA. Phys Rev B 1999;59:3393.
[32] Grochola G, Russo SP, Snook IK. J Chem Phys 2005;123:204719.
[33] Mishin Y, Mehl MJ, Papaconstantopoulos DA, Voter AF, Kress JD. Phys Rev B 2001;63:224106.
[34] Mendelev MI, Sordelet DJ, Kramer MJ. J Appl Phys 2007;102:043501.
[35] Ackland GJ, Tichy G, Vitek V, Finnis MW. Philos Mag A 1987;56:735.
[36] Foiles M, Baskes M, Daw M. Phys Rev B 1986;33:7983.
[37] Angelo J, Moody N, Baskes M. Model Simul Mater Sci Eng 1995;3:289.
[38] Chen SP, Srolovitz DJ, Voter AF. J Mater Res 1989;4:62.
[39] Zimmerman JA, Gao H, Abraham FF. Model Simul Mater Sci Eng 2000;8:103.
[40] Rodney D. Acta Mater 2004;52:607.
[41] Bacon DJ, Osetsky YN, Rodney D. Dislocation-obstacle interactions at the atomic level. In: Hirth JP, Kubin L, editors. Dislocations in solids, vol. 15. Amsterdam: North-Holland; 2009. p. 4 [chapter 88].
[42] Rodney D. Phys Rev B 2007;76:144108.
[43] Mahajan S, Barry DE, Eyre BL. Philos Mag 1970;21:43.
[44] Hirth J, Lothe J. Theory of dislocations. New York: Wiley; 1982.